

Wake of forced flow around elliptical leading edge plates

R. Mills, J. Sheridan, K. Hourigan*

*Fluids Laboratory for Aeronautical and Industrial Research (FLAIR), Department of Mechanical Engineering,
Monash University, Melbourne 3800, Australia*

Received 3 March 2003; accepted 18 October 2004

Available online 17 January 2005

Abstract

Previous investigations have shown that flows around rectangular plates with transverse forcing involve interactions between vortices shed from the leading and trailing edges and vortex merging in the wakes. The Strouhal number of vortex shedding at which peak base drag occurs varies with chord-to-thickness ratio in a stepwise fashion, similar to the self-sustained oscillations at low Reynolds number for unforced flows. In the present study, the leading edge flow separation and vortex shedding is eliminated by using plates with elliptical leading edges, and the trailing edge flow is examined through particle image velocimetry. In particular, the response of the trailing-edge vortex shedding and the base pressure coefficient to applied transverse oscillations of different Strouhal number and amplitude is measured. Substantial variation in the base pressure coefficient is found, with peaks appearing at the natural shedding frequency and at a harmonic. The effect of the forcing on the wake dimension and the strength of the wake vortices is quantified using particle image velocimetry. Three-dimensional structures in addition to the two-dimensional Kármán vortices in the wake are also visualized.

© 2004 Elsevier Ltd. All rights reserved.

1. Introduction

Flows that are globally unstable due to the presence of a region of absolute instability in the wake exhibit self-excited oscillations, and can be categorized as oscillators (Huerre and Monkewitz, 1990). Due to the naturally occurring self-excited instability, they tend to be unresponsive to small amplitude perturbations. Only by applying perturbations of sufficiently high amplitude to effectively alter the mean flow can the flow be controlled by external perturbations.

The Kármán vortex shedding from a circular cylinder is an example of a globally unstable flow. It has a region of absolute instability in the wake, as well as the two separated shear layers that are locally convectively unstable. Karniadakis and Triantafyllou (1989) performed a direct numerical simulation of the flow about a circular cylinder in the presence of a periodic external forcing, and found that the response of the wake could be qualitatively represented by a two-parameter space inside a resonant horn.

Small amplitude flow perturbations near the Kármán shedding frequency have little effect on vortex shedding. For perturbation amplitudes above the minimum threshold, perturbation frequencies within the lock-in boundary result in a near wake with a frequency equal to the perturbation frequency. For perturbation frequencies outside the receptivity boundary, the frequency in the near wake is equal to the natural vortex-shedding frequency, while perturbation

*Corresponding author. Tel.: +61 3 9905 3628; fax: +61 3 9905 9602.
E-mail address: kerry.hourigan@eng.monash.edu.au (K. Hourigan).

Nomenclature

A	area, mm ²
Cp_b	base pressure coefficient defined as $P_{\text{base}}/(\frac{1}{2}\rho U_o^2)$, dimensionless
$Cp_{b_{\text{max}}}$	maximum (negative) base pressure coefficient, dimensionless
Cp_{b_o}	base pressure coefficient for unperturbed flow, dimensionless
C^*L	boundary layer constant, dimensionless
c	plate chord, mm
c/t	plate chord to thickness ratio, dimensionless
d	cylinder diameter, mm
dA	area of image covered by gridpoint, mm ²
f	vortex shedding frequency, Hz
f_e	oscillation frequency, Hz
f_o	natural vortex shedding frequency, Hz
f_p	perturbation frequency, Hz
$F_{t'}$	defined as $0.286 \text{Re}_{t'}$, dimensionless
l_f	vortex formation length, mm
P	pressure, Pa
P_{base}	time averaged base pressure, Pa
P_{rms}	r.m.s. fluctuating pressure, Pa
Re	Reynolds number defined as $U_o t/v$, dimensionless
$\text{Re}_{t'}$	Reynolds number defined as $U_o t'/v$, dimensionless
Re_x	Reynolds number defined as $U_o x/v$, dimensionless
S	distance along body surface, mm
St	Strouhal number defined as ft/U_∞ dimensionless
St_p	perturbation Strouhal number defined as $f_p t/U_\infty$, dimensionless
t	plate thickness, mm
t'	plate thickness + twice boundary layer displacement thickness at separation, defined as $t' = t + 2\delta_*$, mm
u	perturbation velocity, m s ⁻¹
u'	amplitude of perturbation velocity, m s ⁻¹
U_o	free stream velocity, m s ⁻¹
U_x	streamwise component of velocity, m s ⁻¹
U_y	cross-stream component of velocity, m s ⁻¹
x	streamwise distance, mm
y	cross-stream distance, mm also amplitude of body motion, mm
Γ	circulation, m ² s ⁻¹
δ_*	boundary layer displacement thickness at separation, mm
ΔC_p	difference in pressure coefficient between leading and trailing stagnation points, dimensionless
ΔP	difference in pressure between leading and trailing stagnation points, Pa
ν	kinematic viscosity, m ² s ⁻¹
τ	time, s
ω	vorticity, s ⁻¹

Common acronyms used

A/D	analog to digital converter
AC	alternating current
C	Celsius
CFD	Computational Fluid Dynamics
CSIRO	Commonwealth Scientific and Industrial Research Organisation
LDV	Laser Doppler Velocimetry
PIV	Particle Image Velocimetry
r.m.s.	root-mean square
SPL	Sound Pressure Level
β -mode	transverse duct acoustic mode

frequencies within the two regions between the lock-in boundary and the receptivity boundary result in a quasi-periodic wake, with both the perturbation frequency and the natural vortex-shedding frequency present in the wake. Stansby (1976) found a similar response of vortex shedding to transverse oscillations of a circular cylinder in a series of wind tunnel experiments. Vortex shedding from a rectangular trailing edge of a body with an aerofoil leading edge also shows similar response to perturbations compared to a circular cylinder, with a minimum threshold perturbation level required in order for the vortex shedding to be modified (Wu et al., 1993). For perturbation levels above the threshold level, Lotfy and Rockwell (1993) found that a range of frequencies existed near the natural vortex-shedding frequency where perturbations would result in a lock-in state.

To understand better the mechanisms that influence flow induced oscillations of bluff bodies, a common approach is to control the oscillations in order to eliminate the effects of structural damping and the various structural modes of vibration that can exist for a body, allowing oscillation amplitude and frequency to be varied independently [see reviews by Bearman (1984) and Griffin and Hall (1991)]. As with research on flows over stationary bluff bodies, the majority of work has focussed on circular cylinders and other relatively short bluff bodies, with only a few researchers investigating the effects of oscillating elongated bluff bodies.

Stansby (1976) investigated the effect on the base pressure (Cp_b) of a circular cylinder subject to transverse oscillations. He found that the vortex shedding could be phase locked to the cylinder at oscillation frequencies near the natural Strouhal shedding frequency. For a fixed ratio of amplitude of cylinder vibration to cylinder diameter (y/d), as the frequency of oscillation (f_e) was increased past the natural shedding frequency (f_o) of a stationary cylinder, a large phase shift between the cylinder motion and the vortex shedding was observed to coincide with a sudden change in Cp_b .

As the ratio y/d was increased, the size of the change in Cp_b was observed to increase. One other feature that Stansby did not draw attention to is that as y/d is increased, the frequency at which the phase jump in vortex-shedding occurs decreases. Stansby also found that by fixing the separation point at $\pm 70^\circ$ with a thin circular rod, there was no organized effect due to lock on for $y/d = 0.10$, and the value of Cp_b is always close to the value for the stationary cylinder.

The results of Davies (1976) for a D-section cylinder show that for a value of $y/d = 0.2$, with the vortex-shedding phase locked to the cylinder motion, there was an increase of 35% in circulation ($\Gamma/U_o d$) of the shed vortices. Griffin and Ramberg (1975) showed that there is an inverse relationship between the vortex strength in the wake of an oscillating cylinder and the length of the vortex formation region (l_f). The drag coefficient was also found to increase with decreasing vortex-formation length, which is consistent with the findings of Bearman (1967) who studied the effects of base bleed on the drag of stationary bluff bodies.

Nakamura and Hirata (1989) looked at the vortex shedding from oscillating rectangular prisms with chord (c) to thickness (t) ratios $c/t = 0.2-1.0$, subject to vibrations of amplitude $y/t = 0.1$. For all plates tested, perturbations applied near the natural shedding frequency of a stationary rectangular cylinder resulted in the vortex-shedding phase locking to the oscillations. For plates shorter than the critical value of $c/t = 0.6$, where for stationary cylinders the base pressure is a minimum, the application of the oscillations reduced the base pressure. Associated with this was a shortening of the vortex-formation length. The cylinder with $c/t = 0.4$ was found to have the lowest base pressure and thus the highest drag. For the prisms with $c/t > 0.6$, a recovery in base pressure was observed, as the shear layer-trailing edge interaction was enhanced, resulting in an increased radius of curvature of the shear layers and an increase in vortex-formation length. Nakamura and Hirata (1991) showed that both the cylinders with $c/t = 0.4$ and 0.6 showed significant changes in the phase angle between vortex shedding and cylinder oscillation near resonance. Bearman and Obasaju (1982) also observed large changes in the phase angle for square cylinders oscillating with amplitudes $y/t = 0.05$ and 0.1 when the frequency of oscillation was near the natural shedding frequency.

The process of vortex shedding from an oscillating rectangular trailing edge of a long plate fitted with an elliptical leading edge was investigated by Lotfy and Rockwell (1993). Over a relatively narrow frequency range ($0.95 \leq f_e/f_o \leq 1.05$), vortex shedding was observed to be phase locked to the trailing edge oscillations. The term “phase locked” means that the shedding pattern is highly repeatable from cycle to cycle. Over this frequency range, the small changes in f_e/f_o resulted in a change of almost 180° in the phase of vortex formation with regard to the trailing edge motion. Lotfy and Rockwell (1993) used a time clock analogy to explain the differences in phase angle, due to changes in the times required for vortex formation and departure from the trailing edge. For frequencies outside this range ($0.50 \leq f_e/f_o < 0.95$ and $1.05 < f_e/f_o \leq 2.0$), the flow structure is not phase-locked to the trailing edge motion and a modulated flow structure is observed. This is due to mode competition that occurs between the self-excited global instability frequency f_o of vortex shedding for the stationary plate, and the perturbation frequency f_e . The wake frequency is equivalent to f_o , but the flow structure is modulated due to perturbations produced by the edge at the frequency f_e .

For oscillating bluff bodies of various shapes, one common feature is that, over a range of frequencies of oscillation near the natural vortex-shedding frequency of the stationary body, the vortex shedding will synchronize, or phase lock,

with the body motion. The range of frequencies depends strongly on the amplitude of motion of the bluff body or the strength of the external perturbations, and can be as large as $\pm 20\%$ of the natural shedding frequency in extreme cases of body motion or flow perturbation. Over this range of frequencies, large changes in the phase relationship between vortex shedding and body motion can be seen, although the occurrence and nature of the phase shift has been shown to be highly dependent on the afterbody geometry (Ongoren and Rockwell, 1988). Substantial changes in the base pressure coefficient for short bluff bodies are also observed to coincide with this phase change, if there is no interference on the vortex formation from the leading edge by the downstream surfaces of the body. For a bluff body with a significant afterbody length, there is in fact no phase shift in vortex shedding from the leading edge observed as the body oscillation frequency is varied (Ongoren and Rockwell, 1988).

Greenway and Wood (1973) observed resonant shedding from a plate in a duct with an elliptical leading edge and a rectangular trailing edge. They used a towing tank with a similar plate that was oscillated in a direction transverse to the mean flow direction to perform flow visualization experiments and to measure the circulation of vortices shed from the trailing edge using an early form of PIV. When the plate was oscillated at the natural vortex-shedding frequency of a stationary plate, the trailing edge shedding was phase-locked to the oscillations and the circulation of the trailing edge vortex-shedding increased significantly. Flow visualization showed that the correlation of vortex shedding across the span was increased, and the vortices formed closer to the trailing edge of the body.

Blevins (1985) investigated the effect of a transverse sound field on vortex shedding from circular cylinders. The motivation for investigating the effect of sound on vortex shedding was to understand the acoustic feedback that occurs when vortex-induced sound reflects from large stationary surfaces back to the cylinder surface. This sound reflection and feedback mechanism has been reported to be responsible for intense noise and vibration of some tube-and-shell heat exchangers found in large power plants, often at amplitudes high enough to cause structural damage to the heat exchangers. Blevins found that vortex shedding from a cylinder could be phase-locked to an applied sound field over a range of frequencies near the natural shedding frequency of the cylinder. When this happened, the coherence of the vortex shedding across the span increased substantially. As the sound pressure levels applied to the flow about the cylinder were increased, so too was the range of frequencies that the vortex shedding could be phase locked to the sound field. Blevins also found it was the acoustic particle velocity that was responsible for the locking on of vortex shedding at the sound frequency, not the sound pressure fluctuations.

Wu et al. (1993) used a water tunnel with moveable sidewalls to simulate the Parker β -mode acoustic field found in ducts. They investigated the vortex shedding from a plate with an elliptical leading edge and a rectangular trailing edge in the presence of transverse velocity perturbations applied at the natural shedding frequency. As with flows about circular cylinders, there was found to be a minimum perturbation level of 0.35% of free-stream velocity required to phase lock the vortex shedding across the trailing edge of the plate. For natural vortex shedding and with perturbation levels below this threshold, vortex shedding was not well correlated across the span. For perturbation levels above the lock-in threshold level, vortex shedding was well correlated across the span, giving insight into how the resonant sound field reported by Welsh et al. (1984) can enhance vortex shedding.

Previous studies have been undertaken by Mills et al. (2002, 2003) and numerically by Tan et al. (1998, 2004) and Hourigan et al. (2001) on the flow around cylinders with both rectangular leading and trailing edges. It was shown that if the flow around a rectangular cylinder in an open jet wind tunnel is forced by small transverse oscillations, similar in form to a duct resonant acoustic cross mode, a stepwise variation in the frequency at which peak base drag occurs is found as the chord-to-thickness ratio of the cylinder is varied. The vortex shedding at the trailing edge was influenced by both the forcing from the applied oscillations and from interference from the leading edge vortices. The current study seeks to provide an understanding of the effect of forced oscillations alone, through the removal of the vortex shedding at the leading edge by introducing an elliptical leading edge.

2. Experimental method

An open jet wind tunnel was used for surface pressure measurements and flow visualization, while a water tunnel was used for PIV measurements and flow visualization.

2.1. Wind tunnel design

The wind tunnel used was an open jet tunnel which was designed and constructed at the Commonwealth Scientific and Industrial Research Organisation (CSIRO), Melbourne. An open jet wind tunnel was used, rather than a closed wall tunnel, to eliminate the possibility of acoustic resonances that can be excited by vortex shedding from bluff bodies in enclosed ducts (Welsh and Gibson, 1979; Parker, 1997). The main drawback associated with the use of an open jet

tunnel is the inherently higher free-stream turbulence level compared to a conventional enclosed draw-down type tunnel.

The wind tunnel is illustrated in Fig. 1. Air flow is supplied by a centrifugal fan powered by a variable speed AC motor. Flow from the fan passes through a wide angle diffuser containing four perforated plates into a settling chamber containing a honeycomb and four nylon screens. It then passes through an 8:1 contraction into a 244 mm \times 244 mm outlet from which it exits to form a free jet. The tunnel could operate over a jet velocity range of 0–15 m s⁻¹.

Fig. 2 shows the location of the model in the working section, and the loudspeakers either side of the model to generate the transverse velocity perturbation. The loudspeakers were located far enough away from the model so they did not interfere with the mean flow of the tunnel.

The loudspeakers were 12 inch diameter single cone design, with a frequency range of 50 Hz–1 kHz. The speakers were connected in antiphase, and could generate sound pressure levels of 120 dB (re 20 μ Pa) measured at the midchord position on the plate surface, when driven at a frequency of 100 Hz.

The minimum turbulence level measured was 0.25% adjacent to the tunnel exit for velocities between 6 and 12 m s⁻¹. This increased to 1.0% at a distance of 1 outlet diameter downstream, and reached about 2.5% at the furthest point downstream at a distance of 2 outlet diameters. This variation of turbulence level is consistent with that expected of an open jet, and matches closely the results obtained by Michel and Froebel (1988). The leading edge of the experimental models was placed at a distance of 0.6 outlet diameters away from the tunnel outlet. At this point, the free stream turbulence level was 0.30%.

A Scannivalve was used to connect a Setra 239E pressure transducer to pressure tapings on the wind-tunnel models, one at a time. These allowed time average surface pressures to be measured.

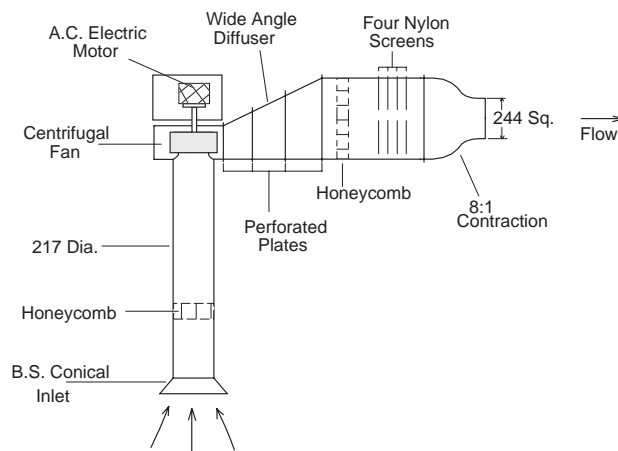


Fig. 1. Schematic of the open jet wind tunnel (all dimensions in mm).

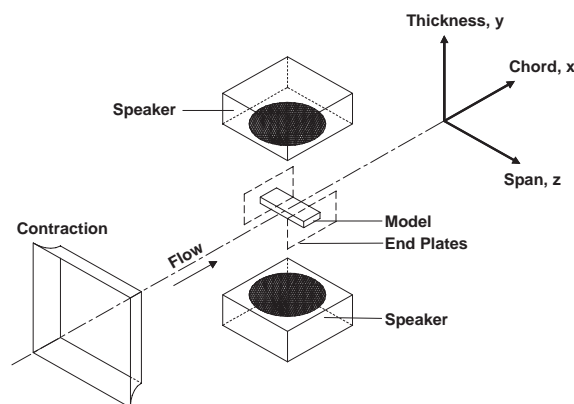


Fig. 2. Schematic of wind tunnel working section.

2.1.1. Wind tunnel models

Wind tunnel models were made from brass, had a nominal thickness of $13 \text{ mm} \pm 0.02 \text{ mm}$, and were 135 mm wide. All models had a C4 aerofoil leading edge profile (Wallis, 1977) and a rectangular trailing edge. This profile was chosen to avoid flow separation at the leading edge. Pressure tapings were placed at regular intervals across the trailing edge to allow the base pressure to be measured. A schematic of a plate cross-section is shown in Fig. 3.

End-plates were constructed from perspex, and were used in all tests. They were 370 mm long, 100 mm high, and 9 mm thick. Their main function was to keep the acoustic field uniform around the model (Parker and Welsh, 1983).

2.1.2. Measurement of transverse perturbation velocity using LDV

In order to allow direct comparison of wind-tunnel data with data obtained from other experimental facilities as well as CFD data, the size of the velocity perturbation applied to the mean flow was measured using a laser-Doppler velocimetry (LDV) system. A TSI system 9100 Helium Neon LDV system configured in a simple forward scatter arrangement was used, with no beam expansion or frequency shifting. A smoke generator was used to produce seeding particles. To achieve a zero mean velocity for the seeding particles in the working section, the entire room containing the wind tunnel was filled with the seeding particles, which were allowed to settle for a period of several minutes. Once the size of the velocity perturbation had been measured, a probe microphone positioned at the midchord position above the plate surface was then used to ensure that the sound pressure level (SPL) for all subsequent tests was held constant. Because the r.m.s. fluctuating pressure (P_{rms}) is directly proportional to the maximum perturbation velocity (Parker and Welsh, 1983), the microphone was used to measure the SPL needed for each experiment to generate velocity perturbations of a required amplitude.

A full description of the wind tunnel experimental set-up can be found in Mills et al. (2002).

2.2. Water tunnel design

The water tunnel used was a low-turbulence closed circuit design, which was designed and constructed at the CSIRO, Melbourne. A schematic of the water tunnel and working section is shown in Fig. 4.

A pump driven by an AC electric motor was used to generate the mean flow in the tunnel test-section. Water was pumped through a diffuser incorporating screens into a settling chamber containing filter material, and a honeycomb section. The water then passed through a two-dimensional four-to-one contraction, with an outlet dimension of $244 \text{ mm} \times 244 \text{ mm}$, into a duct having the same cross-sectional dimensions. The working section had flexibly mounted side-walls to allow a periodic velocity perturbation to be applied in a direction perpendicular to the mean flow. The applied velocity perturbation was similar to that imposed by a resonant acoustic β -mode (Parker, 1966, 1997; Tan et al., 1998). The two 400 mm long moveable sidewalls had glass windows, and were rigidly connected to each other and sealed to the remainder of the test section by a thin flexible membrane. Harmonic oscillations of the sidewalls were produced by a variable-speed drive. The drive was connected to the sidewall support frame via a crank and connecting rod, which allowed a variable stroke. The oscillation amplitude of the sidewalls could be varied from 0 to 5 mm at frequencies between 0 and 6 Hz. A Schlumberger DG5 linear displacement transducer was used to monitor the oscillating test section wall displacements, the output of which was recorded by the computer via an A/D board.

With the perturbations being periodic in nature, the phase of the perturbation cycle is defined relative to the perturbation velocity field as shown in Fig. 5. The sinusoidal perturbation velocity at any time (τ) is given by the function $u(\tau) = u' \sin(2\pi f_p \tau)$, where the phase of the perturbation cycle at any time is equal to $2\pi f_p \tau$. Thus, a perturbation phase angle of 0° gives the perturbation velocity to be zero but about to increase in the upwards direction, while 90° denotes the maximum perturbation velocity in the upwards direction.

The flow velocity (U_o) in the working section could be varied between 0 and 0.4 ms^{-1} , and for the velocities used in the experiments, the mean longitudinal turbulence level was approximately 0.1% of U_o at the tunnel speed of 0.1 m s^{-1} . A full description of the tunnel characteristics is given by Wu et al. (1993).

2.2.1. Water tunnel models

A test-plate was made from clear acrylic; and spanned the 244 mm wide working section of the water tunnel. The plate had a C4 aerofoil leading edge profile (Wallis, 1977) and a chord (c) to thickness (t) ratio, c/t , of 10. The model was located vertically on the centreline of the working section. The water temperature was approximately constant at 15° C for all experiments.

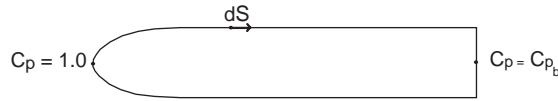


Fig. 3. Schematic of aerofoil leading edge plate profile.

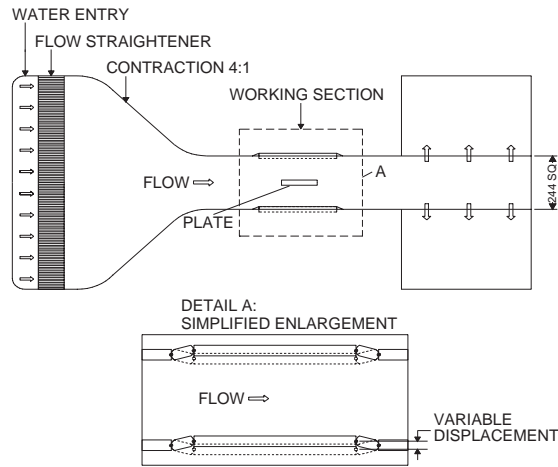


Fig. 4. Schematic of the water tunnel working section (all dimensions in mm).

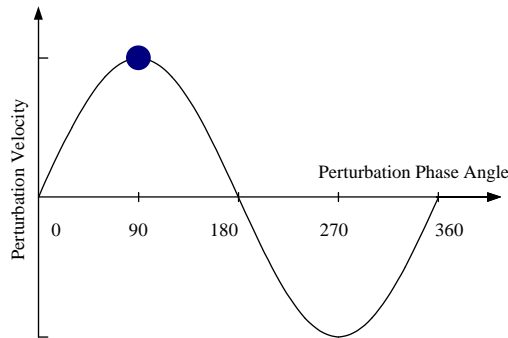


Fig. 5. Graph of perturbation velocity versus perturbation phase angle.

2.2.2. Particle image velocimetry

Instantaneous fluid velocities were measured using the Particle Image Velocimetry (PIV) technique. A full description of the water tunnel experimental setup and PIV technique used is given by Mills et al. (2003). The Reynolds number, Re , for the PIV measurements was 1100 based on plate thickness, corresponding to $U_o = 0.1 \text{ m s}^{-1}$.

2.2.3. Calculation of circulation of vortex structures

The circulation (Γ) of a vortex structure was found by integrating the vorticity (ω) calculated from the discrete velocity data over the area of the vortex (A) according to the formula:

$$\frac{\Gamma}{U_0 t} = \frac{\int_A \omega dA}{U_0 t}, \tag{1}$$

where dA is the area of the image covered by each grid point. The area of a vortex was defined by specifying a central point within the vortex, as well as a rectangular bounding box. All gridpoints within the bounding box were interrogated, with the circulation at gridpoints with vorticity of the same sign as and no less than 10% of the vorticity at

central point being added to the circulation of the entire vortex. The circulation was normalized by the free stream velocity (U_o), and the model thickness (t).

3. Results and discussion

Experimental measurements were taken of the flow around elongated plates with rectangular trailing edges, and both aerofoil and rectangular leading edges. Surface pressure measurements and smoke wire visualizations were taken using the open jet wind tunnel described in Section 2.1, while PIV measurements and flow visualisation images were taken in the closed circuit water tunnel described in Section 2.2.

For long plates with aerofoil leading edges and rectangular trailing edges, there is no vortex shedding from the leading edge of the models. The boundary layers that form on each side of the models separate from the sharp corners at the trailing edge, and interact to form a Kármán vortex street.

3.1. Surface pressure measurements

For the unforced flow case, the variation of the base pressure coefficient, C_{p_b} , with c/t ratio is shown in Fig. 6, measured in the wind tunnel with the flow velocity at 10 m s^{-1} .

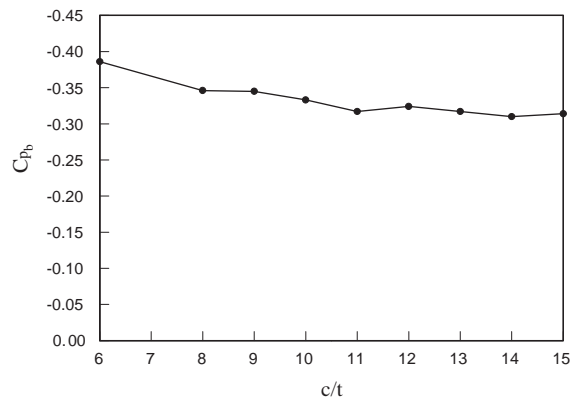


Fig. 6. Variation of C_{p_b} with c/t for a plate with an aerofoil leading edge and a rectangular trailing edge with $t = 13 \text{ mm}$ and $U_o = 10 \text{ m s}^{-1}$ (unforced case).

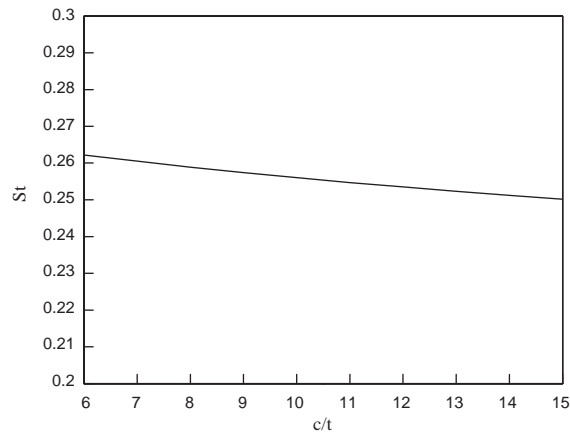


Fig. 7. Predicted variation in St with c/t using Eqs. 2–5 to predict shedding frequency and thus St , for a plate with an aerofoil leading edge and a rectangular trailing edge with $t = 13 \text{ mm}$ and $U_o = 10 \text{ m s}^{-1}$.

Bull and Pickles (1995) showed that the vortex-shedding frequency from such plates depends on the boundary layer state at the plate trailing edge. For a laminar boundary layer at separation, the effect of increasing plate length is to thicken the boundary layers at separation, which results in a wider wake and thus a lower Strouhal number St . Fig. 7 shows the calculated variation in St with c/t for plates with thickness (t) of 13 mm and a flow velocity of 10 m s^{-1} , and assuming a laminar boundary layer at separation, using the following formula from Bull and Pickles (1995):

$$f = vF_{t'}/t'^2, \quad (2)$$

where

$$F_{t'} = 0.286\text{Re}_{t'}, \quad (3)$$

$$\text{Re}_{t'} = U_o t' / \nu \quad (4)$$

and δ_* (used in the calculation of t') was calculated using the relationship

$$\frac{\delta_*}{x} = \frac{C_{*L}}{\text{Re}_x^{1/2}} \quad (5)$$

with $x = c$, and $C_{*L} = 1.7208$ for a laminar boundary layer.

As for a stationary circular cylinder in smooth flow, as St decreases so does the magnitude of Cp_b (Williamson, 1996).

For a plate with a thickness (t) of 13 mm, $c/t = 10$ and a flow velocity of 10 m s^{-1} , the vortex shedding frequency (f) calculated with Eq. (2), gives a vortex shedding Strouhal number $St = 0.256$ based on plate thickness.

3.1.1. Effect of transverse velocity perturbations on Cp_b

Fig. 8 shows the variation of Cp_b with perturbation Strouhal number (St_p) for a plate with $c/t = 10$, a flow velocity of 10 m s^{-1} , and a perturbation level (u'/U_o) of 5%. The variation of Cp_b with St_p is remarkably similar to that observed by Stansby (1976) for a transversely oscillating circular cylinder. Stansby associated the sudden change in Cp_b with a large shift in the phase of vortex shedding with respect to the cylinder motion.

Lotfy and Rockwell (1993) performed a series of experiments on a model with an elliptical leading edge, and a trailing edge that could be oscillated transversely. They found that vortex shedding could be phase-locked to the trailing edge oscillations over the relatively narrow frequency range $0.95 \leq f_e/f_o \leq 1.05$ (where f_e = oscillation frequency and f_o = natural vortex-shedding frequency from a stationary model). Within this frequency range, a small change in f_e/f_o resulted in a change of almost 180° in the phase of vortex formation with regard to the trailing edge motion. This suggests the possibility that the large change in Cp_b when St_p is near the natural vortex shedding St of 0.24 in Fig. 8 coincides with a large change in the phase of vortex shedding with respect to the transverse velocity perturbations.

For plates of different c/t ratios, a similar response to transverse perturbations of the same magnitude is observed, as shown in Fig. 9. Due to the variation of Cp_b with c/t when no perturbation is applied, the value of Cp_b for each plate length without perturbations applied has been subtracted from the data.

The only effect of increasing plate length is thicker boundary layers at separation as discussed in 3.1, so the relative independence of the Cp_b data from c/t shown in Fig. 9 is not surprising.

3.1.2. Effect of varying perturbation level

Since varying the plate length has little effect on Cp_b as St_p is varied, only the effect of perturbation level on Cp_b for the plate with c/t ratio of 10 is presented in Fig. 10. As the relative perturbation level is increased, the size of the maximum change in Cp_b from the unperturbed flow value increases, as is shown in Fig. 11. This result is similar to that observed by Stansby (1976) for flow around a circular cylinder subject to forced transverse oscillations, where increasing the oscillation amplitude resulted in an increased change in Cp_b . Also consistent with the results of Stansby is the reduction in frequency at which the sudden change in Cp_b occurs as the relative perturbation level is increased. Further study is needed to establish whether the sudden change in Cp_b as St_p is increased is due to the flow suddenly phase-locking to the perturbations, or if it is due to already phase-locked vortex shedding undergoing a large phase shift relative to the perturbation cycle.

3.1.3. Effect of higher frequency perturbations

Fig. 12 shows the effect on Cp_b of applying perturbations at St_p as high as 0.9 for the plate with c/t ratio of 10. As already discussed in this section, the natural vortex shedding St is approximately 0.25, and there is a peak in base suction when perturbations are applied at this frequency due to vortex-shedding phase-locking to the perturbations. A second (small) peak in base suction occurs when St_p is approximately 0.5, which is twice the natural vortex-shedding frequency. A third (larger) peak in base suction is observed when St_p is approximately 0.75, which is three times the

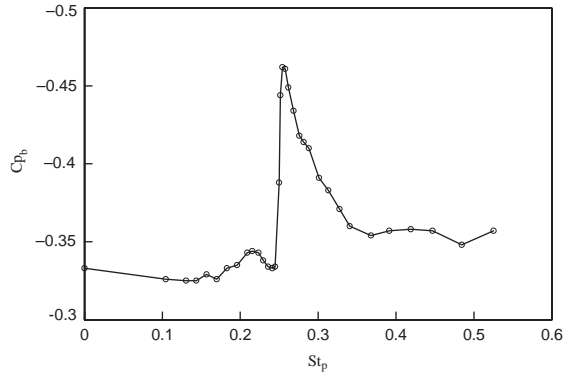


Fig. 8. Variation of C_{p_b} with St_p for $u'/U_o = 5\%$ and $U_o = 10 \text{ m s}^{-1}$ and $c/t = 10$.

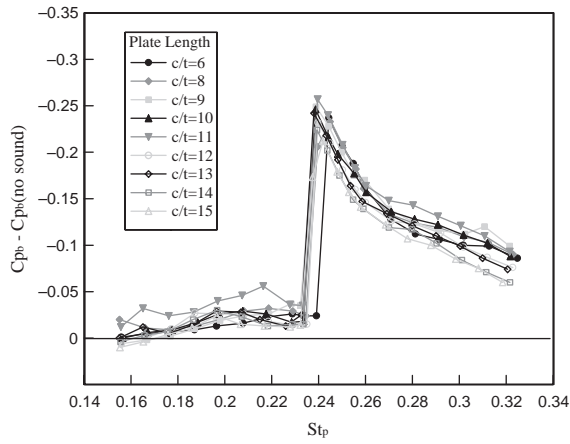


Fig. 9. Variation of change in C_{p_b} from C_{p_b} with no perturbation applied for different length plates, all with $U_o = 10 \text{ m s}^{-1}$ and perturbation level $u'/U_o = 5\%$.

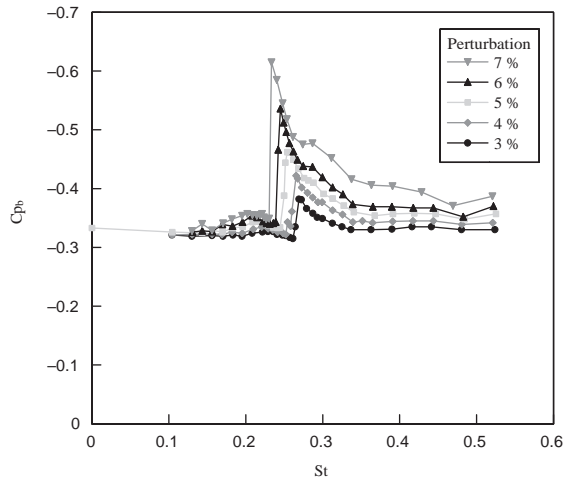


Fig. 10. Effect of perturbation level, u'/U_o , on C_{p_b} for the plate with $c/t = 10$.

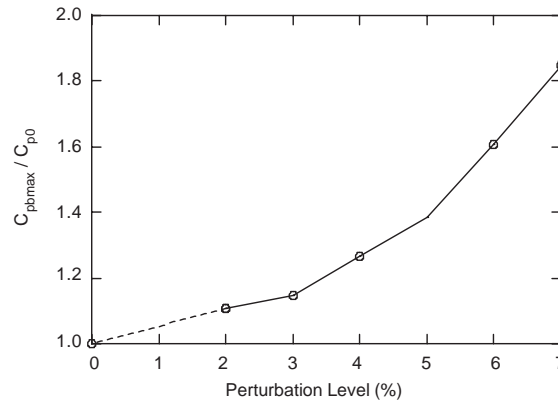


Fig. 11. Variation of $C_{pb_{max}}/C_{pb_0}$ with perturbation level for a $c/t = 10$ plate.

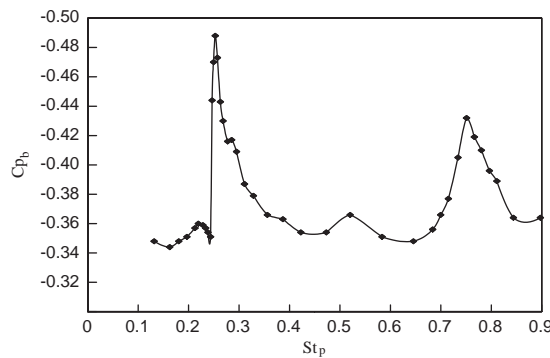


Fig. 12. Variation of C_{pb} with St_p for the plate with $c/t = 10$ and perturbation level $u'/U_o = 5\%$.

natural vortex shedding St . Flow visualisation revealed that large-scale vortex shedding occurred at approximately $St = 0.25$, a subharmonic of the perturbation frequency when perturbations were applied at $St_p = 0.75$. The vortex shedding appeared enhanced by the perturbations, which was expected given the increased base suction measured in the wind tunnel.

3.2. Particle image velocimetry measurements

Using PIV in the water tunnel, the effect of transverse velocity perturbations on the vortex shedding from the rectangular trailing edge of an aerofoil leading edge plate has been investigated. The aim of the PIV experiments was to gain insight as to why the large pressure drops measured in the wind tunnel experiments occur; in particular, to identify variations in the formation or location of flow structures. The Reynolds number for all PIV experiments on the aerofoil leading edge plate was 1100 based on plate thickness.

3.2.1. No transverse velocity perturbations

Fig. 13 shows velocity, sectional streamlines and vorticity fields, for a plate without transverse perturbation applied. The velocity vector plot, Fig. 13(a), and the corresponding sectional streamline plot, Fig. 13(b), were both generated with a stationary reference frame with respect to the laboratory, while the sectional streamline plot, Fig. 13(c), was generated with the reference frame moving at $0.75 U_o$, approximately the convection velocity of the vortices. Vortices of opposite sign are shed alternately from the trailing edge to form a vortex street. This is clearly evident in the vorticity plot (Fig. 13(d)). The frequency of vortex shedding, calculated by measuring the time of 20 shedding cycles, was found to be 1.80 Hz. This gave a natural vortex shedding St of approximately 0.25, in close agreement with Bull and Pickles (1995), as discussed earlier.

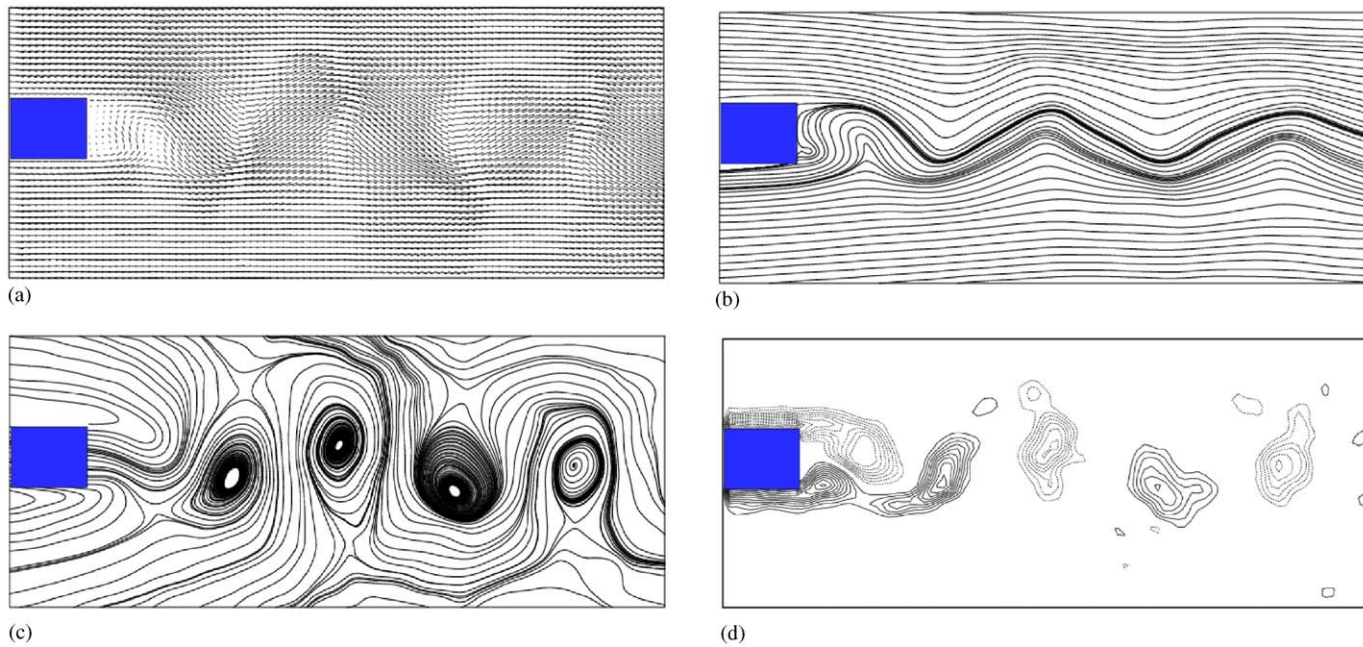


Fig. 13. PIV results on flow around a plate with an aerofoil leading edge ($c/t = 10$, $Re = 1100$), without any perturbation applied. (a) velocity vector plot, (b) sectional streamlines (lab reference frame), (c) sectional streamlines (reference frame moving with vortices), (d) vorticity (solid line, clockwise; dotted line, counter-clockwise).

Fig. 14 shows a plot of the vertical velocity U_y against streamwise distance from the centre of the trailing edge; the wavelength of vortex shedding is seen to be approximately $4.0t$.

A total of 10 PIV images were processed for the aerofoil leading edge model without any transverse velocity perturbation. Profiles of U_x were extracted from the PIV data at several streamwise locations and averaged, as shown in Fig. 15. These velocity profiles show a top hat profile at the trailing edge. As x/t increases the wake spreads and the size of the velocity deficit decreases.

3.2.2. Transverse velocity perturbation applied

PIV measurements were made on flow about a plate with an aerofoil leading edge in the presence of a 6% transverse sinusoidal velocity perturbation. Fig. 16 shows plots of velocity, sectional streamlines and vorticity when the movable sidewalls used to generate the transverse velocity perturbation were in the lowest position. This corresponds to a phase angle of 0° , with a perturbation velocity of 0. The perturbation frequency was 1.65 Hz, giving $St_p = 0.235$. For this perturbation level, this was the lowest perturbation frequency for which the vortex shedding was phase-locked to the perturbation. This corresponds to the St_p for which the largest change in C_{pb} was observed for a 6% velocity perturbation (see Fig. 10).

Comparing the vorticity plots of Figs. 13(d) and 16(d), it can be seen that the spacing between vortices is reduced in the presence of the transverse perturbations, indicating a reduced convection velocity of vortices when phase-locked to the perturbations. Fig. 17 shows a plot of U_y/U_o against streamwise distance from the centre of the trailing edge. This image shows the wavelength of vortex shedding to be approximately $3.8t$. If the convection velocity of vortices remained unaffected by the application of transverse perturbations, then the spacing between vortices when $St_p = 0.235$ should be $4.26t$. With a 6% transverse velocity perturbation applied at the lowest perturbation frequency that results in phase-locked vortex shedding, the convection velocity of vortices is only 89% of that for vortices shed from the model when no perturbation is applied. This is consistent with the findings of Davies (1976) for a transversely oscillating circular cylinder, where oscillating the cylinder at the natural vortex-shedding frequency of the stationary cylinder increased the circulation of the shed vortices by 35%, and reduced the convection velocity to only 90% of the convection velocity of vortices shed from a stationary cylinder.

A total of 8 PIV images were processed for the aerofoil leading edge model with a 6% transverse velocity perturbation applied. The images selected were separated by 45° intervals in the perturbation cycle. It is recognized that a single image at each phase point is not sufficient to obtain a statistically significant average of the velocity data for that phase angle. However, profiles of U_x were extracted from the PIV data at several streamwise locations and averaged as shown in Fig. 18, and are useful in indicating the size of the velocity deficit in the wake.

Comparing Fig. 16(a) with Fig. 13(a), it is seen that the region behind the trailing edge representing slow moving or reversed flow is much smaller when the flow is perturbed. This would suggest that the vortex-formation length is smaller when vortex shedding is phase-locked to the perturbation field, an expected result given the higher base suction (see Fig. 9) and the observations of other researchers as discussed in the Introduction.

3.2.3. Relationship between circulation and base pressure

Eq. (6) shows that the rate of circulation formation at a point on a surface is equal to the pressure drop along that surface (Morton, 1984), as indicated in Fig. 3:

$$\int \frac{d\Gamma}{d\tau} dS = - \int \frac{\partial P}{\partial S} dS. \quad (6)$$

By integrating along either the upper or lower surface from the leading edge to the centre of the trailing edge, the rate of circulation generation about the entire model is equal to the change in pressure from the stagnation point at the leading edge to the trailing edge, as shown in Eq. (7):

$$\frac{d\Gamma}{d\tau} = -\Delta P. \quad (7)$$

Integrating Eq. (7) over the period of one entire vortex-shedding cycle gives

$$\frac{\Gamma}{\Delta P} = \text{constant}. \quad (8)$$

For two different cases (1 and 2) of flow about a model like the one shown in Fig. 3, the relationship between circulation in the wake and pressure change about the surface of the model is given by Eq. (9):

$$\frac{\Gamma_1}{\Gamma_2} = \frac{\Delta P_1}{\Delta P_2} = \frac{\Delta C_{p1}}{\Delta C_{p2}}. \quad (9)$$

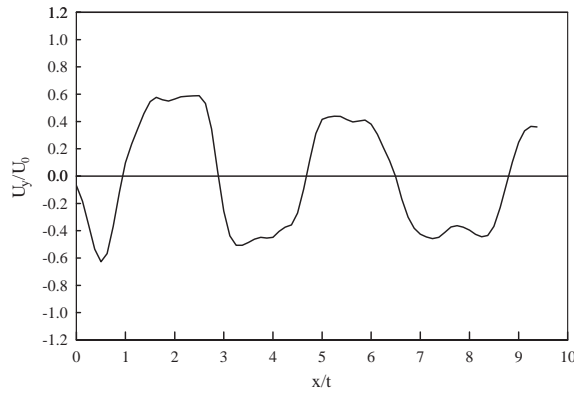


Fig. 14. Variation of U_y/U_o with streamwise distance from the trailing edge (x/t) for the plate with c/t ratio of 10.

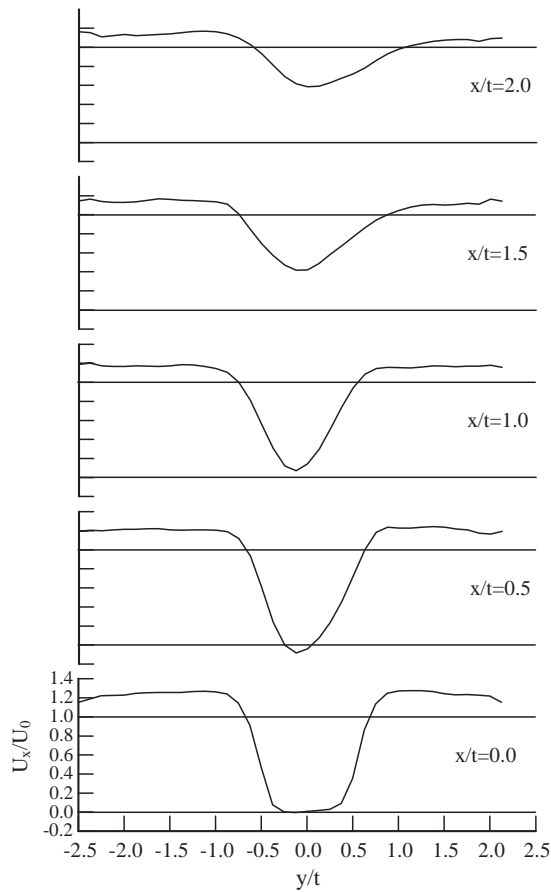


Fig. 15. Variation of U_x velocity profile across the wake with streamwise distance (x/t), with no transverse velocity perturbation applied for the plate with c/t ratio of 10.

Fig. 19 shows the variation of circulation with streamwise distance from the trailing edge of the aerofoil leading edge model, both with and without transverse velocity perturbations applied.

Using the least-squares lines of best fit through the two sets of data shown in Fig. 19 to extrapolate back to the trailing edge of the model, the circulation of vortices in the wake adjacent to the trailing edge is given in Table 1. Also

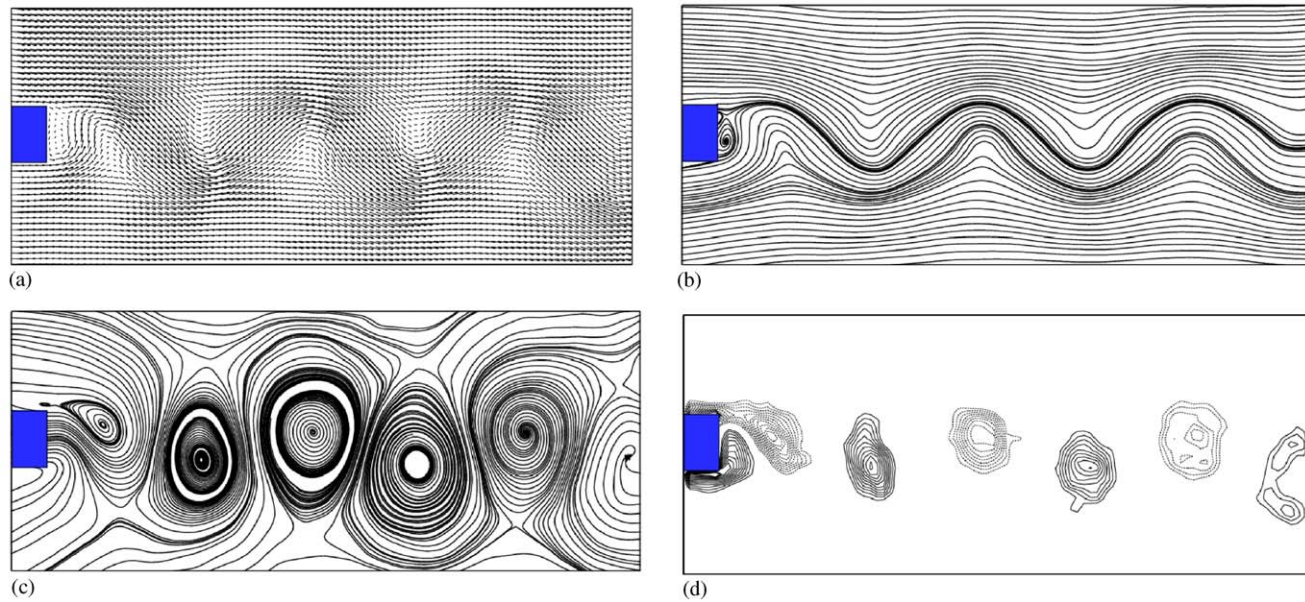


Fig. 16. PIV results of wake for the flow around a plate, $c/t = 10$, with an aerofoil leading edge ($Re = 1100$), with 6% transverse velocity perturbation applied at $St_p = 0.235$: (a) velocity vector plot, (b) sectional streamlines (lab reference frame), (c) sectional streamlines (reference frame moving with vortices), (d) vorticity (solid line, clockwise; dotted line, counter-clockwise). Perturbation phase = 0° .

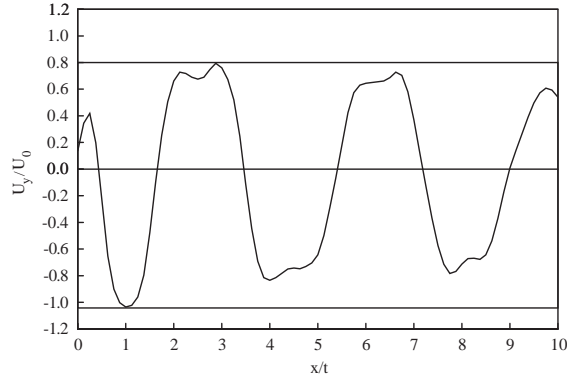


Fig. 17. Variation of U_y/U_o with streamwise distance from the trailing edge (x/t) for the plate with $c/t = 10$ and $U_o = 0.1 \text{ m s}^{-1}$.

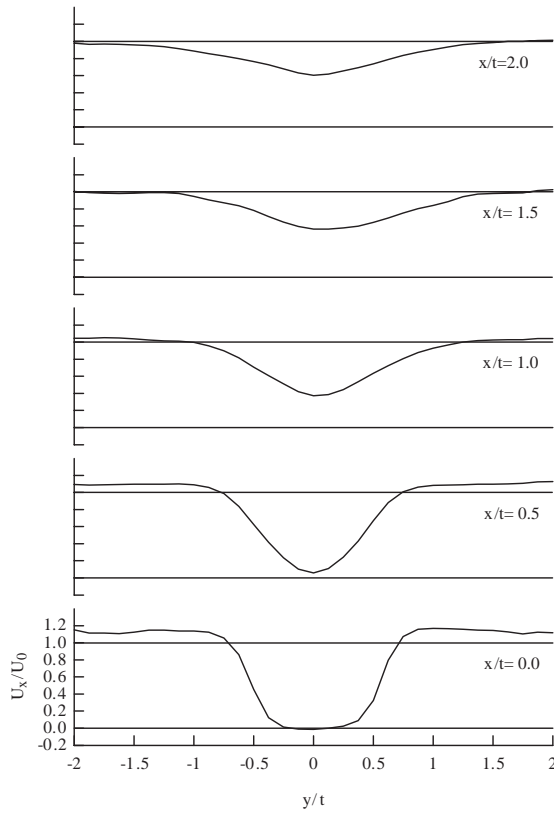


Fig. 18. Variation of U_x average velocity profile across the wake with streamwise distance (x/t), 6% transverse velocity perturbation applied at $St_p = 0.235$ for the plate with $c/t = 10$ and $U_o = 0.1 \text{ m s}^{-1}$.

shown in Table 1 is the change in pressure coefficient from the stagnation point at the leading edge of the model to the base of the model, both for the case of no transverse velocity perturbation applied, and for the case when a 6% transverse velocity perturbation is applied at $St_p = 0.235$.

Using Eq. (9), the expected base pressure coefficient in the presence of a 6% velocity perturbation applied at $St_p = 0.235$ is -0.552 . This is within 3% of the base pressure coefficient measured in the wind tunnel. Although the response to perturbations of only one level has been measured in the water tunnel, this result indicates that the extra

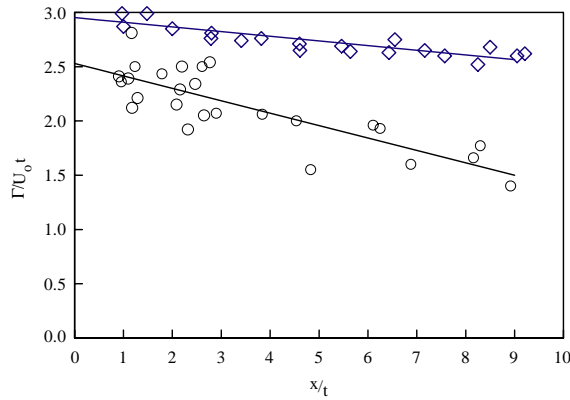


Fig. 19. Variation of normalized circulation with streamwise distance (x/t) from the trailing edge of a plate, $c/t = 10$, with an aerofoil leading edge: $-\diamond-$, with 6% velocity perturbation applied at $St_p = 0.235$; $-o-$, natural vortex shedding. Lines represent least-squares lines of best fit.

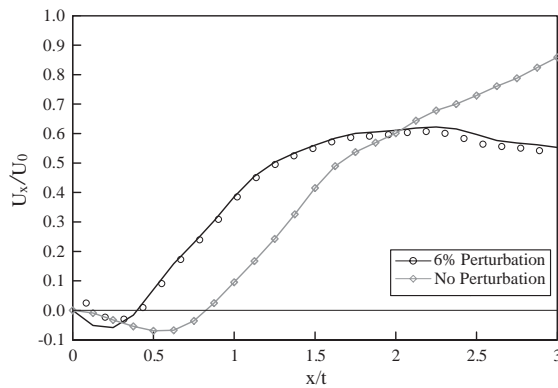


Fig. 20. Variation of streamwise component of velocity (U_x/U_0) with streamwise distance from the centre of the trailing edge of a plate, $c/t = 10$, with an aerofoil leading edge.

Table 1

Comparison between circulation shed from a bluff body and the pressure change around it

Circulation	Γ_1/Γ_2	ΔCp	$\Delta Cp_1/\Delta Cp_2$
$\Gamma_1 = 2.53$	0.857	$\Delta Cp_1 = 1.33$	0.866
$\Gamma_2 = 2.95$		$\Delta Cp_2 = 1.54$	

circulation present in the wake when vortex shedding is phase-locked to transverse velocity perturbations corresponds with the large drop in base pressure.

There are other factors that can affect the base pressure of a bluff body. Bearman (1965) established that the base pressure is also directly affected by the vortex-formation length. As the formation length decreased so did the base pressure, resulting in higher drag. The vortex-formation length is often defined as the streamwise location along the centreline of the wake where the velocity fluctuations measured by a hot-wire are a maximum. With only 10 PIV images being processed for each case, there are not sufficient data to obtain an accurate estimate of formation length using this definition. However, Fig. 20 shows the variation of U_x (average at each streamwise location for all PIV images) with streamwise distance (x/t) along the centreline of the wake for the case without any transverse perturbation applied and with a 6% transverse velocity perturbation applied. The region of reverse flow is smaller in the presence of transverse velocity perturbations, indicating that the formation length is reduced.

3.3. Three-dimensional effects

The base pressure measurements and PIV results presented to date may give the impression that the vortex shedding from the trailing edge of a plate with an aerofoil leading edge is two-dimensional (2-D). For flow over circular cylinders, three-dimensional (3-D) effects are observed for Re greater than 190 (Williamson, 1996), although Wu et al. (1996) found evidence of 3-D structures at $Re = 170$ which may be a function of free stream turbulence and end-effects. Wu et al. (1996) found that the circulation of streamwise vortices associated with mode B vortex shedding (Williamson, 1996) in the wake of a circular cylinder was only 11% of the circulation of the spanwise vortices. Wu et al. (1996) also found evidence of similar streamwise vortices in the wake of a plate with a semi-circular leading edge and a rectangular trailing edge, so it was expected that there would be streamwise structures in the wake of models with aerofoil leading edges. Fig. 21 shows a flow visualization image taken in the water tunnel of vortex shedding from a plate with an aerofoil leading edge and a rectangular trailing edge. The sheet of laser light was aligned to reveal the classical 2-D Kármán vortices in the wake. A feature of the flow that was not expected to be seen using this technique was the existence of streamwise vortices embedded in the Kármán vortex street.

The PIV vorticity plot shown in Fig. 22 was generated from an image taken with the sheet of laser light aligned to reveal streamwise vortex structures. When vortex shedding was locked to transverse velocity perturbations, the streamwise structures appeared to be suppressed, although no PIV data has been processed showing this; this would be worthy of further investigation. The intention of drawing attention to the existence of 3-D structures in the flow is not

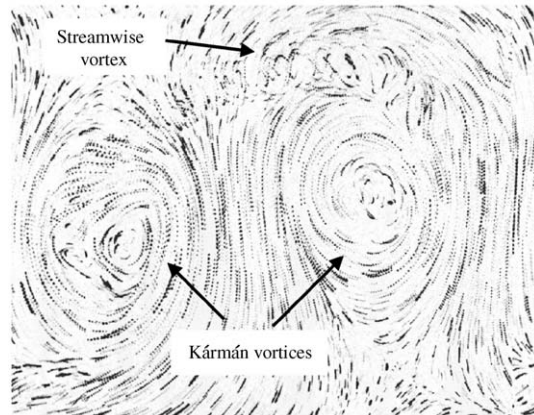


Fig. 21. Short time particle traces of vortex shedding from the rectangular trailing edge of a plate, $c/t = 10$, with an aerofoil leading edge showing streamwise vortex superimposed on primary spanwise Kármán vortices, no perturbation applied. Flow is from left to right.

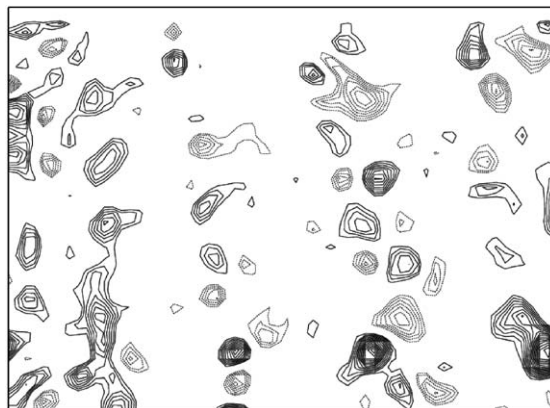


Fig. 22. Vorticity contour plot, with the laser sheet orientated in the same plane as the plate, $c/t = 10$, to reveal streamwise vortex structures across the span of the wake. Flow is from left to right.

to draw any conclusion about the effect of three dimensionality on vortex shedding or C_{p_b} , but rather to acknowledge that 3-D structures are present.

Nonparallel vortex shedding also results in the formation of 3-D structures. Williamson (1989) showed that end-conditions were responsible for nonparallel vortex shedding from circular cylinders, and Pickles and Bull (1992) showed that parallel vortex shedding from models with aerofoil leading edges and rectangular trailing edges was also dependent on end conditions. Although vortex shedding from the base of a model with a semi-circular leading edge was regular in the absence of transverse velocity perturbations, Wu et al. (1993) showed that it was not well correlated across the span, indicating that the shedding was nonparallel. When transverse velocity perturbations were applied at a frequency close to the natural vortex-shedding frequency, and at an amplitude sufficiently high to lock the vortex shedding to the perturbations, the vortex shedding was found to be well correlated across the span of the model (Wu et al., 1993), and therefore parallel.

4. Conclusions

Previous studies by the researchers have concentrated on the complex vortex interactions that occur in flows around long rectangular plates. The flow around plates with rectangular trailing edges and elliptical leading edges have been studied here to isolate the trailing edge vortex shedding and the effect of transverse flow perturbations.

The base suction was measured for models with aerofoil leading edges and rectangular trailing edges. In the absence of any externally applied perturbations, the base suction was found to decrease slightly as the c/t ratio was increased. This is due to a thickening of the laminar boundary layer at separation, resulting in a wider wake and a lower vortex shedding St .

Flow visualization and PIV measurements in the water tunnel showed that the natural vortex shedding has a strong streamwise component of vorticity that is only weakly correlated across the span, consistent with the studies of the wake of a circular cylinder by Wu et al. (1993, 1996).

In another set of experiments, finite amplitude transverse velocity perturbations were superimposed on the mean flow. As the perturbation frequency was increased the base suction remained almost constant before suddenly increasing to a maximum at a frequency just below the natural vortex-shedding frequency (f_o). The size of the peak in base suction was found to increase with increasing perturbation level, while the perturbation frequency at which the jump in base suction occurred was found to decrease with increasing perturbation level. As the perturbation frequency was raised above f_o , the base suction was observed to recover to a value close to that found when no perturbations were applied.

A second small peak in base suction was found to occur when the perturbation frequency equalled $2f_o$, while another large peak was measured as the perturbation frequency approached $3f_o$. When the perturbation frequency was equal to $3f_o$, large-scale vortex shedding was observed to occur at a frequency close to the natural shedding frequency (f_o), a subharmonic of the perturbation frequency.

When perturbations were applied at a frequency close to f_o , flow visualizations showed that vortex shedding was phase-locked to the velocity perturbations at the frequency and perturbation level that resulted in a peak value of base suction. PIV results showed that the increase in base suction coincides with increased circulation of the vortices shed from the trailing edge, and a reduction in vortex-formation length. Another factor contributing to the higher base suction was the increase in spanwise correlation of vortex shedding when it was phase-locked.

Due to the absence of vortex shedding from the leading edge, the frequency at which peak values of base suction occurred showed only a weak dependence on c/t ratio. Vortex shedding at the trailing edge was found to be dependent on the state of the boundary layer at separation, as well as the frequency and amplitude of any applied transverse velocity perturbations.

Acknowledgements

Dr Richard Mills acknowledges the support of an Australian Post Graduate Scholarship and use of the facilities at CSIRO Building, Construction and Engineering, Melbourne.

References

Bearman, P.W., 1965. Investigation of the flow behind a two-dimensional model with a blunt trailing edge and fitted with splitter plates. *Journal of Fluid Mechanics* 21, 241–255.

- Bearman, P.W., 1967. The effect of base bleed on the flow behind a two-dimensional model with a blunt trailing edge. *Aeronautical Quarterly* 18, 207–224.
- Bearman, P.W., 1984. Vortex shedding from oscillating bluff bodies. *Annual Review of Fluid Mechanics* 16, 195–222.
- Bearman, P.W., Obasaju, E.D., 1982. An experimental study of pressure fluctuations on fixed and oscillating square-section cylinders. *Journal of Fluid Mechanics* 119, 297–321.
- Blevins, R.D., 1985. The effect of sound on vortex shedding from cylinders. *Journal of Fluid Mechanics* 161, 217–237.
- Bull, M.K., Li, Y., Pickles, J.M., 1995. Effects of boundary layer transition on vortex shedding from thick plates with faired leading edge and square trailing edge. *Proceedings of 12th Australasian Fluid Mechanics Conference*, pp. 231–234.
- Davies, M.E., 1976. A comparison of the wake structure of a stationary and oscillating bluff body, using a conditional averaging technique. *Journal of Fluid Mechanics* 75, 209–231.
- Greenway, M.E., Wood, C.J., 1973. The effect of a bevelled trailing edge on vortex shedding and vibration. *Journal of Fluid Mechanics* 61, 323–335.
- Griffin, O.M., Hall, M.S., 1991. Review-Vortex shedding lock on and flow control in bluff body wakes. *ASME Journal of Fluids Engineering* 113, 526–537.
- Griffin, O.M., Ramberg, S.E., 1975. On vortex strength and drag in bluff-body wakes. *Journal of Fluid Mechanics* 69, 721–728.
- Hourigan, K., Thompson, M.C., Tan, B.T., 2001. Self-sustained oscillations in flows around long blunt plates. *Journal of Fluids and Structures* 15, 387–398.
- Huerre, P., Monkewitz, P.A., 1990. Local and global instabilities in spatially developing flows. *Annual Review of Fluid Mechanics* 22, 473–537.
- Karniadakis, G.E.M., Triantafyllou, G.S., 1989. Frequency selection and asymptotic states in laminar wakes. *Journal of Fluid Mechanics* 199, 441–469.
- Lotfy, A., Rockwell, D., 1993. The near wake of an oscillating trailing edge: mechanisms of periodic and aperiodic response. *Journal of Fluid Mechanics* 251, 173–201.
- Michel, U., Froebel, E., 1988. Lower limit for the velocity fluctuation level in wind tunnels. *Experiments in Fluids* 6, 45–54.
- Mills, R., Sheridan, J., Hourigan, K., 2002. Response of base suction and vortex shedding from rectangular prisms to transverse forcing. *Journal of Fluid Mechanics* 461, 25–49.
- Mills, R., Sheridan, J., Hourigan, K., 2003. Particle Image Velocimetry and flow visualisation of natural and forced flow around rectangular cylinders. *Journal of Fluid Mechanics* 478, 299–323.
- Morton, B.R., 1984. The generation and decay of vorticity. *Geophysical and Astrophysical Fluid Dynamics* 28, 277–308.
- Nakamura, Y., Hirata, K., 1989. Critical geometry of oscillating bluff bodies. *Journal of Fluid Mechanics* 208, 375–393.
- Nakamura, Y., Hirata, K., 1991. Pressure fluctuations on oscillating rectangular cylinders with the long side normal to the flow. *Journal of Fluids and Structures* 5, 165–183.
- Ongoren, A., Rockwell, D., 1988. Flow structure from an oscillating cylinder Part 1. Mechanism of phase shift and recovery in the near wake. *Journal of Fluid Mechanics* 191, 197–223.
- Parker, R., 1966. Resonance effects in wake shedding from parallel plates: some experimental observations. *Journal of Sound and Vibration* 4, 62–72.
- Parker, R., 1997. Aeroacoustics. *International Journal of Fluid Dynamics* 1, Article 1, (<http://elecpress.monash.edu.au/ijfd>).
- Parker, R., Welsh, M.C., 1983. Effects of sound on flow separation from blunt flat plates. *International Journal Heat and Fluid Flow* 4, 113–128.
- Pickles, J.M., Bull, M.K., Li, Y., 1992. Effects of boundary layer transition on vortex shedding from thick plates with faired leading edge and square trailing edge. *Proceedings 11th Australasian Fluid Mechanics Conference*, pp. 31–34.
- Stansby, P.K., 1976. Base pressure of oscillating cylinders. *Proceedings of ASCE Journal of Engineering Mechanics* 102, 591–600.
- Tan, B.T., Thompson, M.C., Hourigan, K., 1998. Flow around long rectangular plates under cross flow perturbations, *International Journal of Fluid Dynamics* 2, Article 1, (<http://elecpress.monash.edu.au/ijfd>).
- Tan, B.T., Thompson, M.C., Hourigan, K., 2004. Flow past rectangular cylinders: receptivity to transverse forcing. *Journal of Fluid Mechanics* 515, 33–62.
- Wallis, R.A., 1977. The F-series aerofoils for fan blade sections. *The Institute of Engineers Australia, Mechanical Engineering Transactions*, pp. 12–20.
- Welsh, M.C., Gibson, D.C., 1979. Interaction of induced sound with flow past a square leading edge plate in a duct. *Journal of Sound and Vibration* 67, 501–511.
- Welsh, M.C., Stokes, A.N., Parker, R., 1984. Flow-resonant sound interaction in a duct containing a plate, Part I: Semi-circular leading edge. *Journal of Sound and Vibration* 67, 510–511.
- Williamson, C.H.K., 1989. Oblique and parallel modes of vortex shedding in the wake of a circular cylinder at low Reynolds numbers. *Journal of Fluid Mechanics* 206, 579–627.
- Williamson, C.H.K., 1996. Vortex dynamics in the cylinder wake. *Annual Review of Fluid Mechanics* 28, 477–539.
- Wu, J., Sheridan, J., Soria, J., Welsh, M.C., Hourigan, K., 1993. Experimental investigation of vortex shedding from a plate: effect of external velocity perturbation. *Journal of Wind Engineering and Industrial Aerodynamics* 49, 401–410.
- Wu, J., Sheridan, J., Welsh, M.C., Hourigan, K., 1996. Three-dimensional vortex structures in a cylinder wake. *Journal of Fluid Mechanics* 312, 201–222.